electronics

MDPI

Article

A Versatile Platform for PV System Integration into Microgrids

Gabriel Gómez-Ruiz [1,*], Reyes Sánchez-Herrera [1], Jesús Clavijo-Camacho [1], Juan M. Cano [2], Francisco J. Ruiz-Rodríguez [1] and José M. Andújar [1]

[1] Research Centre CITES, University of Huelva, 21007 Huelva, Spain; reyes.sanchez@dfaie.uhu.es (R.S.-H.); jesus.clavijo@die.uhu.es (J.C.-C.); javier.ruiz@die.uhu.es (F.J.R.-R.); andujar@uhu.es (J.M.A.)
[2] Department of Electrical and Thermal Engineering, Design and Projects, University of Huelva, 21007 Huelva, Spain; juan.diaz@die.uhu.es
* Correspondence: gabriel.gomez@diesia.uhu.es

Abstract: Advancing decarbonization critically depends on the integration of PV systems into microgrids. However, this integration faces challenges, including the variability of photovoltaic solar energy production, the demands of energy management, and the complexities of grid synchronization and communication. To address these challenges, a PV emulator platform is an essential tool. This paper presents a novel four-layer PV emulator platform that seamlessly integrates power systems, control systems, measurement instrumentation, and communication processes. The proposed platform enables the emulation of I-V curves and the dynamic adjustment of operating points—including both the maximum power point (MPP) and power reserve point (PRP)—as well as temperature and irradiance while providing sufficient power capacity for microgrid integration. To validate its effectiveness, the platform was assessed for its capability to adjust operating points, such as MPPs or PRPs, under varying irradiance and temperature conditions. The results show that the platform effectively adjusts operating points with a deviation of less than 5% from theoretical values and successfully tracks a sequence of operating points. This performance underscores the platform's potential in integrating and managing PV systems within microgrid environments, thereby advancing the path to decarbonization.

Keywords: maximum power point tracking; microgrid; photovoltaic emulator; power reserve

Citation: Gómez-Ruiz, G.; Sánchez-Herrera, R.; Clavijo-Camacho, J.; Cano, J.M.; Ruiz-Rodríguez, F.J.; Andújar, J.M. A Versatile Platform for PV System Integration into Microgrids. *Electronics* **2024**, *13*, 3995. https://doi.org/10.3390/electronics13203995

Academic Editor: Carlos Andrés García-Vázquez

Received: 3 September 2024
Revised: 4 October 2024
Accepted: 9 October 2024
Published: 11 October 2024

1. Introduction

Fossil fuels remain the dominant energy source, contributing to 75% of greenhouse gas emissions [1]. To ensure a sustainable future, a shift in the electricity generation mix is imperative. In line with the EU's goal of achieving climate neutrality by 2050 [2], this shift will increasingly rely on low-carbon sources, including renewable energy sources (RESs) and nuclear power. Due to ongoing promotion, RESs have gradually expanded their share, reaching an estimated 23% of the global energy mix in 2023 [3]. Among these, solar energy is particularly crucial on the path to decarbonization. It harnesses the sun, the most abundant energy source, and can be utilized for both thermal and electrical energy through photovoltaic (PV) systems, serving a wide range of energy consumers, from residential homes to industrial facilities. In addition, the integration of these systems into microgrids is crucial for enhancing the sustainability and efficiency of power generation [4,5]. In summary, photovoltaic solar energy, known for being clean, low-maintenance, and increasingly accessible due to rapid technological advancements, has become one of the most mature and widely adopted RESs today [6].

Thus, focusing on PV systems, advancements in key research areas have driven significant and sustained growth. As a result, a wide variety of applications is now available. For instance, PV power plants have gained popularity in recent years due to their increasing capacity for power generation [7]. In addition, PV modules are now commonly installed on the rooftops of residential and commercial buildings, primarily to reduce

electricity costs [8]. However, generating energy to meet energy consumption demands is not the only purpose of PV systems. They are also employed in various innovative applications, such as producing green hydrogen through water electrolysis [9] or powering water desalination systems [10], among others.

Basically, a PV module consists of an aggregation of PV cells, with the output power of each cell influenced by the technology chosen, temperature and irradiance conditions, and shading. Recent advancements in PV cell technology have concentrated on developing new materials and manufacturing techniques, as well as the mathematical models that represent their operational principles.

Accurate mathematical models are crucial for effectively reproducing PV performance curves, specifically the current–voltage (I-V) and power–voltage (P-V) curves. These models allow engineers and researchers to predict the behavior of PV cells at various operating points, defined by specific values of power, irradiance, and temperature, all of which are influenced by the specific application and configuration of the PV installation. Widely used models include the 1M3P (one model, three parameters) and the 1M5P (one model, five parameters) [11]. The 1M5P stands out because it incorporates additional parameters, providing a more accurate representation of the electrical behavior of a PV solar cell compared to the simpler 1M3P model. These models serve as excellent tools for predicting the performance of PV modules in any location, avoiding the physical, climatic, and economic limitations associated with real-world studies [12,13].

After modeling the PV module, the next step involves controlling its operating point, defined by its power, irradiance, and temperature values. This control is critical when the PV module is integrated into a microgrid, as it significantly enhances the system's flexibility in managing energy. In this context, the operating point of a PV module can be either the maximum power point (MPP), representing the highest achievable output, or a power reserve point (PRP), which is set above the MPP. Targeting specified PRPs is crucial for participating in power reserve scenarios, particularly when energy storage systems are not available. In addition, targeting PRPs is essential in applications where the optimal operating point is not the MPP, such as in certain innovative applications previously mentioned.

Effective algorithms are essential to control the operating point. Traditionally methods such as Perturb and Observe (P&O) [14], Incremental Conductance (IncCond) [15], and Constant Voltage (CV) [16] enable continuous adjustments. Although traditionally used for MPP tracking, these algorithms can also be adapted to target other operating points like PRPs. The P&O method periodically adjusts the reference voltage, which is the initial setting for each iteration of the control algorithm, and observes its effect on power output to determine the operating point. The IncCond method, by comparing incremental changes in current and voltage, predicts the direction to the operating point more accurately than P&O, especially under rapidly changing conditions, although it is more complex and computationally demanding. The CV method maintains a fixed reference voltage close to the operating point voltage, minimizing adjustments and simplifying the control system, but may struggle with significant environmental changes. Furthermore, advanced methods such as fuzzy logic-based control algorithms can provide enhanced dynamic response and accuracy; however, their implementation tends to be more complex and demanding [4,5]. Given its balance of simplicity, speed, and efficiency, the P&O method is often favored in practical applications where rapid response and ease of use are priorities [17].

However, rigorous testing under varying conditions is essential to ensure the effectiveness of algorithms that control the operating point of a PV module. Real-world studies involving actual PV modules and natural conditions have significant limitations, as previously mentioned. An alternative approach involves conducting studies in a laboratory setting using actual PV modules, where temperature, irradiance, and shading conditions are controlled. However, this setup is not without challenges—it is complex, costly, and inefficient due to the large area required for the PV modules and the reliance on artificial lighting.

To overcome these challenges, PV emulators offer an effective solution by replicating the electrical characteristics, specifically the I-V curve, of a PV module or an array of modules under various conditions. These devices not only facilitate the modeling and control of PV systems but also serve as essential tools in academic settings, helping in the teaching of the principles and control strategies of PV systems [18].

In summary, PV emulators simulate the behavior of real PV modules, providing researchers and engineers with a flexible, cost-effective, and efficient solution to test and refine their applications without the need for physical PV modules or the complexities of varying environmental conditions.

PV emulators can be categorized into several types, each with distinct characteristics and applications. Analog PV emulators use analog circuitry to replicate the I-V characteristics of PV modules, offering simplicity and cost-effectiveness but limited flexibility [19]. Digital PV emulators rely on microcontrollers or digital signal processors (DSPs) to model PV behavior, providing greater flexibility and the ability to simulate complex scenarios; however, this approach involves higher costs and complexity [20]. Hybrid PV emulators combine analog and digital approaches, aiming to balance performance with flexibility, though they tend to be more complex and costly [21]. Real-time PV emulators are advanced systems designed for high accuracy and dynamic response, making them particularly useful for testing systems under rapidly changing conditions, but they are the most expensive and complex to implement [22]. Each of these emulator types is based on specific devices that align with their intended function, ranging from simple analog components in analog emulators to microcontrollers and DSPs in digital emulators, a combination of both in hybrid emulators, and high-performance processors and real-time systems in real-time emulators.

Among digital PV emulators, those based on programmable power supplies are valued for their balance of simplicity and flexibility, although they tend to be costly. These emulators offer a practical solution for testing and developing PV systems by accurately replicating the characteristics of PV modules without the need for physical solar panels [23].

However, when the objective extends beyond simple replication to include testing within a microgrid scenario—an essential step for promoting the integration of PV systems into microgrids—more complex features are required from a PV emulator, including critical functions such as measurement, control, and communication. To address this, the use of a multi-layered platform that incorporates the PV emulator, along with measurement instrumentation, control systems, and communication processes, is crucial. This setup should enable precise control of the operating point, allowing the system to operate not only at the MPP but also at specified PRPs, which is essential for participating in power reserve scenarios, particularly when energy storage systems are not available. In addition, it should offer a controlled environment for dynamically adjusting temperature and irradiance values.

While the literature on PV emulator platforms has made significant contributions, it also reveals several notable limitations. Firstly, most existing PV emulator platforms are designed for low-power applications and are therefore not suitable for microgrid integration, which typically requires higher power levels in the range of kilowatts [24–26]. Secondly, PV emulator platforms primarily focus on reproducing experimental I-V and P-V curves, but they often fail to address dynamic changes in three critical parameters: operating point, temperature, and irradiance [27–29]. Although a PV emulator based on artificial neural networks and piecewise-linearization techniques, as proposed in [30], introduces dynamic changes in irradiance, temperature, shading, and load, it does not fully incorporate adjustments to the PV array's operating point, such as tracking the MPP or PRP. Moreover, the current literature lacks a comprehensive approach that provides insights into a platform integrating power systems, control systems, measurement instrumentation, and communication processes. This platform would facilitate dynamic adjustments in operating points, temperature, and irradiance conditions for high-power applications intended for microgrid integration.

After analyzing the state of the art concerning PV emulator platforms in the literature, it was concluded that existing platforms lack the necessary measurement, control, and communication capabilities required for in-depth dynamic adjustment of operating points, temperature, and irradiance in high-power applications. This gap, demonstrated in Table 1, motivated the development of the PV emulator platform described in this paper.

Table 1. Comparison of key features in PV emulation platforms identified in the literature. In this table, an 'X' denotes that a platform possesses a particular feature as cited in a reference, while a '-' means the absence of that feature in the reference.

Ref.	Reproducing I-V and P-V Curves	Dynamic Changes in Operating Points, Temperature, and Irradiance	Power Capacity for Microgrid Integration
[24]	X	Only in irradiance	-
[25]	-	-	-
[26]	X	-	X
[27]	X	-	-
[28]	X	-	-
[29]	X	-	-
[30]	X	Only in temperature and irradiance	-
The proposed platform	X	X	X

This paper presents a PV emulator platform that provides a solution for integrating PV systems into microgrids or directly connecting them to the grid. It efficiently manages various operating points, including the MPP and specified PRPs. The platform features a four-layer architecture that seamlessly integrates power systems, control systems, measurement instrumentation, and communication processes, allowing for the precise emulation of PV systems under controllable temperature and irradiance conditions. In addition, the inclusion of a BESS emulator and the ability to follow sequences of operating points further enhance the platform's capability to dynamically manage energy within a microgrid. The platform also serves as an invaluable academic tool for teaching the operational principles of PV systems, their modeling, control, and integration into microgrids. In addition, the platform can also be used for developing components for PV systems, such as PV inverters [31].

Table 1 provides a comparative overview of the key features identified in the discussed literature, including the emulation of I-V and P-V curves, the dynamic changes in operating points, temperature, and irradiance, as well as the power capacity for microgrid integration. This table highlights the strengths and weaknesses of each reference, illustrating how the proposed platform successfully achieves all these critical features, thereby filling the identified research gap.

Based on everything discussed in this section, this paper is novel for the following reasons:

(1) The proposed platform facilitates the integration of PV systems into microgrids, offering a robust testing and development environment from the supplier's perspective.
(2) It can emulate a wide range of PV systems, delivering output power according to specific environmental conditions. This versatility is crucial in scenarios with diverse energy consumers, such as residential houses and industrial facilities.
(3) The platform not only emulates but also facilitates the integration of PV systems within a microgrid, whether operating at the MPP or in power reserve mode at the specified PRP. This functionality is ensured by a microgrid interface (MGI) that allows the MGS to specify the desired operating point, along with an adapted control algorithm that targets this point. Both are seamlessly integrated into a robust communication layer.

In addition, the platform is characterized by the following key features:

(1) An Integrated Four-Layer Architecture: the platform incorporates four essential layers—power, control, measurement, and communication—enabling precise control over the PV array's operating points under varying environmental conditions.
(2) Dynamic Testing Environment: by efficiently managing sequences of operating points and incorporating a BESS emulator, the platform provides a robust environment for microgrid testing.
(3) Advanced Control and Communication: The platform features sophisticated control algorithms and communication protocols. These elements are comprehensively detailed, enhancing the interaction between the hardware components and the MGI, thereby significantly advancing the state of the art in PV emulation.

The rest of the paper is organized as follows: Section 2 outlines the theoretical framework, experimental setup, and methodology employed in developing and evaluating the PV emulator platform. Section 3 explores the platform's four-layer architecture, detailing the roles of each component. Section 4 presents the results from the experimental setups conducted. The paper concludes with Section 5, which discusses the implications of the findings, and Section 6, which summarizes the contributions of this study to renewable energy research and offers insights into the developed platform.

2. Materials and Methods

The materials and methods used in this work are divided into two distinct subsections. The first subsection establishes the theoretical framework for the platform's components that supply, convert, and store energy, including the PV array emulator, the DC-DC boost converter, and the BESS. The second subsection details the setup of these emulated components within the platform and the methodologies applied to evaluate the platform's performance, which includes a custom-designed experimental setup specifically built for this analysis.

Furthermore, the platform is developed in accordance with the methodologies presented in [32], and its communication system design draws on insights from previous studies [33,34].

2.1. Theoretical Framework of Power Systems in the Developed Platform

A deep understanding of the underlying concepts and the roles of the aforementioned components is crucial for a full appreciation of the platform's functionality, as well as for the thorough analysis of the experimental results.

2.1.1. Photovoltaic Module: Characteristics and Modeling

The PV array emulator functions as a generation source by emulating a PV module, which converts sunlight into electricity using semiconductor materials such as silicon (Si), cadmium telluride (CdTe), and copper indium gallium selenide (CIGS), among others [35]. The performance of a PV module is primarily characterized by its I-V and P-V curves, reflecting how voltage, current, and power output vary with changes in irradiance and temperature.

In this work, a five-parameter model (I_{ph}, n, I_0, R_s, and R_{sh}), known as 1M5P, is used to describe the I-V curve under varying irradiance and temperature conditions [11]. In this model, each cell is represented by a current source in parallel with a diode, incorporating both series resistance R_s and shunt resistance R_{sh}, as illustrated in Figure 1.

According to this model, the output current I of the PV cell can be expressed as follows (1) [11]:

$$I = I_{ph} - I_0 \left(e^{\frac{q(V + IR_s)}{nkT}} - 1 \right) - \frac{V + IR_s}{R_{sh}} \quad (1)$$

where I and V represent the output current and voltage of the PV cell, respectively; I_{ph} is the photocurrent generated by sunlight; I_0 is the diode saturation current; q is the electron charge ($q = 1.602 \times 10^{-19}$ C); n is the ideality factor of the diode; k is the Boltzmann constant ($k = 1.3806503 \times 10^{-23}$ J/K); and T is the temperature of the cell.

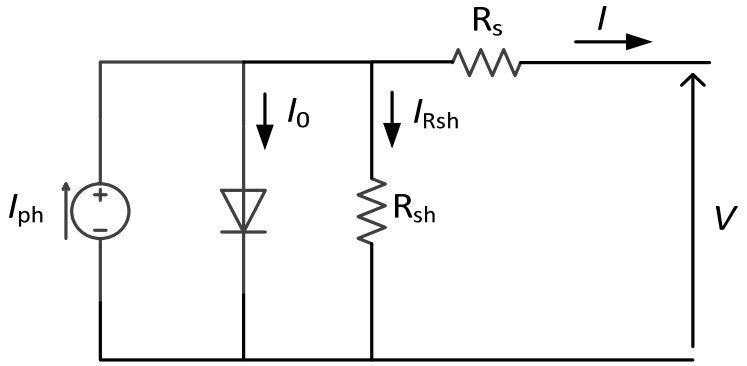

Figure 1. Electrical equivalent circuit using the 1M5P model.

The parameters I, V, I_{ph}, I_0, R_s, and R_{sh}, as outlined in (1), are depicted in Figure 1 to facilitate understanding. Among these, I_{ph}, I_0, n, R_{sh}, and R_s must be determined, typically through optimization techniques, such as the one employed in this work [36]. This technique utilizes data on technical characteristics, temperature coefficients, and environmental conditions to ensure the above parameters are accurately fitted to the provided PV module data. Once this process is completed, I is plotted against V for the specified values of T and G, resulting in the I-V curve for the PV module.

The I-V curve that emerges from this modeling helps identify critical points like the open-circuit voltage V_{oc} and short-circuit current I_{sc}.

2.1.2. DC-DC Boost Converter and Operating Point Tracking

A DC-DC boost converter facilitates continuous adjustment of the operating point of the PV array. In this work, a hybrid control strategy is employed, combining a Proportional–Integral (PI) control approach for the DC/DC boost converter with an adapted P&O algorithm for the PV emulator. The PI controller generates the control signal for the DC/DC boost converter to effectively regulate the output voltage, while the P&O algorithm dynamically adjusts the voltage reference to track the operating point of the PV array. This control strategy was chosen because it aligns well with the characteristics of the experimental microgrid proposed and prioritizes energy efficiency while maintaining a relatively simple implementation. Further details about this control strategy are provided in Section 3.3. Changes in environmental conditions, particularly irradiance and temperature, as well as shifts in the operating point—whether at the MPP or a PRP—affect the control signal and, consequently, the performance of the PV array. In summary, the DC-DC boost converter is essential for maintaining the desired operating point under varying temperature and irradiance conditions, enabling the PV array to operate across its full range and facilitating the acquisition of I-V and P-V curves.

2.1.3. Battery Energy Storage System

A BESS is essential for maintaining a fixed voltage at the output of the DC-DC boost converter in isolated systems. The effectiveness of a BESS is monitored through two key indicators: the State of Charge (*SOC*) and the State of Health (*SOH*).

The *SOC*, which indicates the current energy level of the battery, is calculated using (2):

$$SOC(t) = SOC(0) + \frac{1}{C_{nom}} \int_0^t \left(I_{charge}(\tau) - I_{discharge}(\tau) \right) d\tau \quad (2)$$

where $SOC(0)$ is the initial state of charge, C_{nom} is the nominal capacity of the battery, and $I_{charge}(\tau)$ and $I_{discharge}(\tau)$ are the charging and discharging currents, respectively, over time τ, defined in the interval $[0, t]$.

The *SOH*, which represents the battery's overall condition and its efficiency in storing and releasing energy, is evaluated using (3):

$$SOH = \frac{C_{actual}}{C_{nom}} \times 100 \quad (3)$$

where C_{actual} is the current actual capacity of the battery, and C_{nom} is the nominal capacity.

2.2. Experimental Setup and the Platform's Evaluation Methodology

In this subsection, the setup for the emulated components in the platform and the procedure for evaluating the platform's performance are described.

First, the emulated components include the PV array and the BESS. The PV array was implemented using a unidirectional DC power supply configured to emulate the characteristics of the selected PV array but is versatile enough to represent a wide range of PV systems. The specific characteristics of the PV module are presented in Table 2.

Table 2. Technical characteristics of the selected PV module.

Parameter	Value
N_{cell}	36
V_{oc}	22.7 V
I_{sc}	2.9 A
V_{mpp}	18.3 V
I_{mpp}	2.73 A
α_{Voc}	−0.29506%/°C
β_{Isc}	0.08558%/°C

N_{cell} represents the number of cells per module, V_{mpp} and I_{mpp} denote the voltage and current at the maximum power point, respectively, and α_{Voc} and β_{Isc} are the temperature coefficients for the open-circuit voltage and short-circuit current, respectively.

To design the selected PV array, a setup of 10 panels in series and two panels in parallel was used. This setup was selected to achieve a power output at MPP of approximately 1 kW, with the corresponding voltage and current values detailed in Table 3. In configurations like these, which generate high levels of output power, both the complexity of development and the cost of equipment tend to increase [37–39].

Table 3. PV array configuration. The MPP value is defined by the voltage and current at MPP and is given for T = 25 °C and I = 1000 W/m^2.

Parameter	Value
Series PV Panels	10
Parallel PV Strings	2
MPP	(183 V, 5.46 A)

Note that the parameters depicted in Tables 2 and 3 represent the necessary input for the optimization technique employed to determine the I-V curve of the selected PV array.

Next, the BESS was implemented using a bidirectional power supply, reproducing the behavior of a 350 V Li-Ion battery. The voltage and current characteristics of the Li-ion batteries were configured using the EA® Battery Simulator v2.04 software, which acted as a Battery Management System (BMS). The voltage lower cutoff was set to 2.8 V, and the voltage upper cutoff to 4.2 V, with a layout of 94 batteries in series and one battery in parallel to achieve the mentioned voltage (350 V). In addition, key indicators such as *SOC* and *SOH* were monitored and managed using the software provided by the manufacturer.

3. Developed Platform for PV System Integration into Microgrids

This section provides a detailed description of the developed platform, including its components, their roles, and how they interact. It also includes details about the algorithms implemented for data collection, control, and communication. The development of the platform that follows is based on the fundamental concepts outlined in Section 2.1.

As shown in Figure 2, the platform comprises four distinct layers, each fulfilling a specific role and establishing interactions between the different components of the platform.

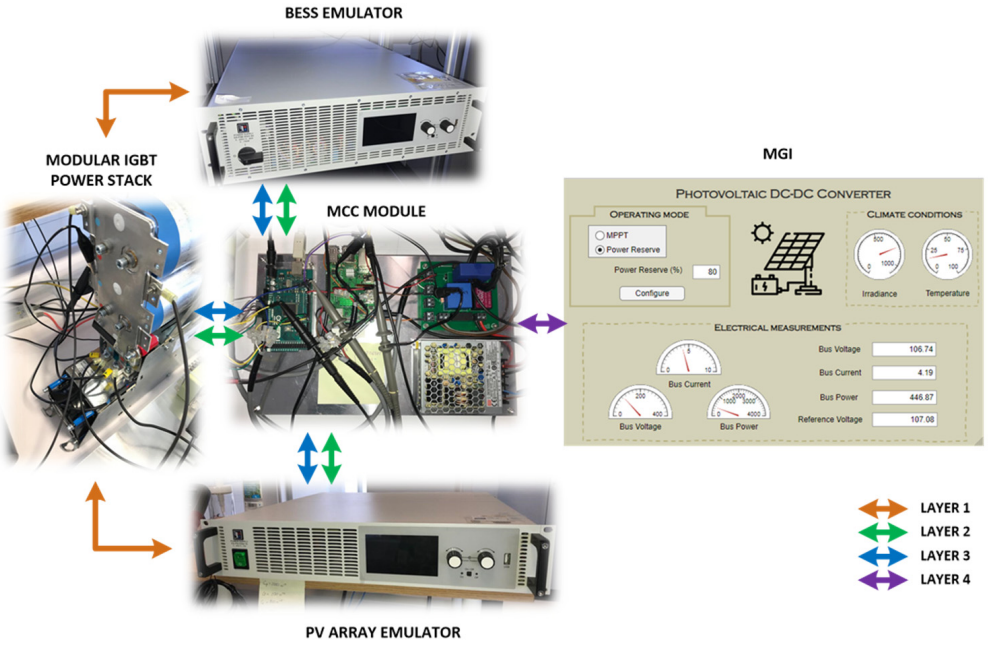

Figure 2. Components of the platform for the characterization of PV arrays illustrating the four layers and their interactions. The four layers are layer 1 (power), layer 2 (measurement), layer 3 (control), and layer 4 (communication).

Layer 1 consists mainly of the power systems that supply, convert, and store energy in the platform. This includes a unidirectional DC power supply acting as a PV array emulator, a DC/DC boost converter for power management, and a bidirectional DC power supply functioning as a BESS emulator. Layer 2 encompasses the measurement components, such as voltage and current sensors, which are crucial for monitoring and control. Layer 3 includes the control system, featuring an acquisition and control board that ensures the PV array emulator operates at any point within its performance curves, i.e., I-V and P-V curves. Finally, Layer 4 involves the communication board and an MGI for configuration and monitoring. All components involved in Layers 2, 3, and 4 are set in the measurement, control, and communication (MCC) module, as shown in Figure 2. This module includes the Data Communication Board (DCB), the Data Acquisition and Control Board (DACB), and the sensors necessary for the measurement process. The functions, components, and processes involved in each layer are described below.

3.1. Layer 1: Power

Layer 1 features a customized circuit, as shown in Figure 3, comprising a PV array emulator, a DC/DC boost converter, a BESS emulator, and other electrical components such as a resistor (R), an inductor (L) and a capacitor (C). The DC/DC boost converter serves as a link between the generation source (PV array emulator) and the storage (BESS emulator) and is essential for several reasons. Firstly, it regulates the voltage by stepping up the output from the PV array emulator to match the voltage required by the BESS emulator, which, in this case, is 350 V. Moreover, the DC/DC boost converter facilitates tracking of

specified operating points, ensuring the PV array emulator functions effectively across all performance curves.

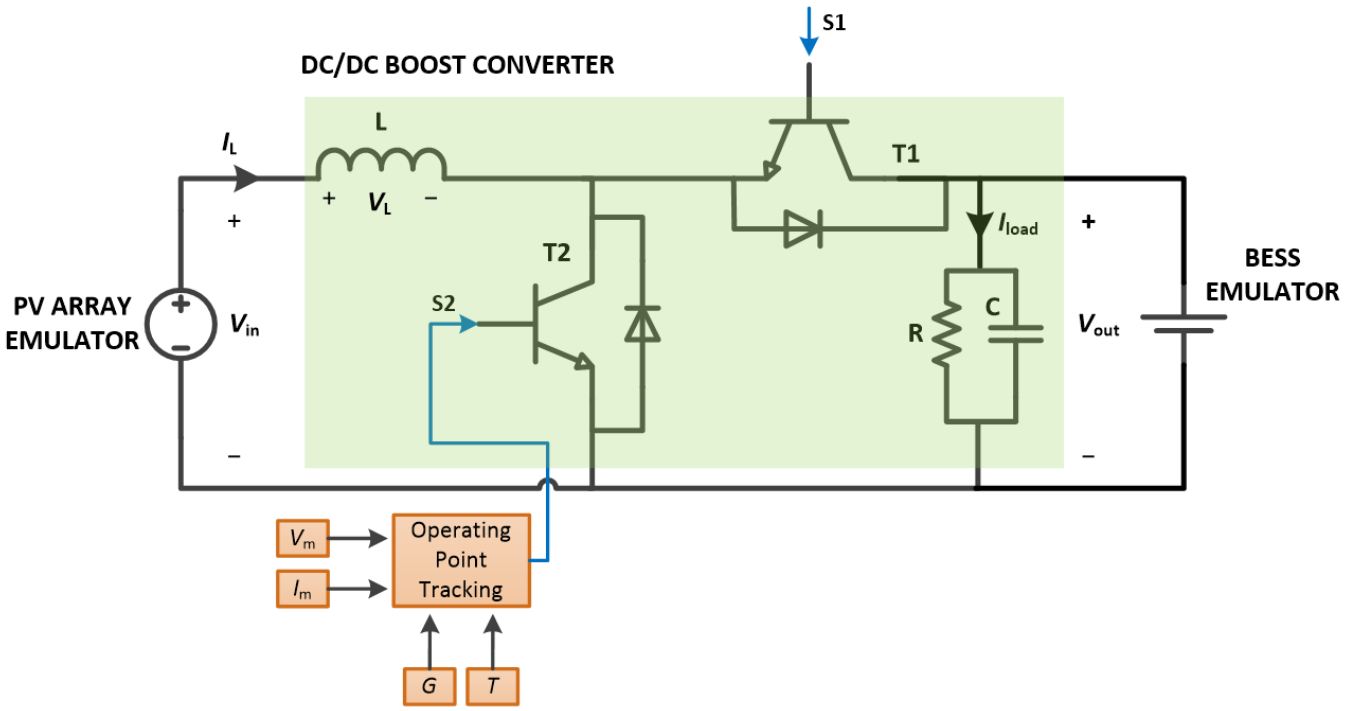

Figure 3. Schematic diagram of the integration of the PV array emulator, the DC/DC boost converter, and the BESS emulator. S1 indicates the fixed signal that keeps transistor T1 open. S2 indicates the control signal coming from the operating point tracking process to transistor T2.

A power supply from the EA®-PSI 9360-15 series (EA® Elektro-Automatik, Viersen, Germany) [40] was selected as the PV array emulator. This initial use of a power supply to emulate the real behavior of PV arrays provides an approach for testing and development. However, the next objective will be to replace the emulator with actual PV arrays.

The output from the PV array emulator is connected to a custom-built DC/DC boost converter featuring a modular IGBT power stack with reference MTM-1/2B2IC0225F12HB (GUASCH®, Barcelona, Spain) [41]. This converter includes two IGBTs (T1 and T2); in this configuration, T1 remains open due to a fixed signal (S1), while T2 is driven by a control signal (S2). The modular IGBT power stack is complemented by a resistor (R), an inductor (L), and a capacitor (C) to build the DC/DC boost converter, with values detailed in Table A1 of Appendix A.

Modeling the circuit depicted in Figure 3 focuses on the dynamic behavior of the DC/DC boost converter under various operational conditions. Given that T1 remains open, the behavior of T2 significantly influences the circuit dynamics. When T2 is on, the inductor charges from the input, resulting in an inductor voltage V_L as defined by (4):

$$V_L = V_{in} \tag{4}$$

Here, V_{in} represents the input voltage from the PV array emulator.

Conversely, when T2 is off, the inductor discharges to the output, leading to the voltage at the inductor and the rate of change in inductor current as outlined in (5) and (6):

$$V_L = V_{in} - V_C \tag{5}$$

$$L\frac{dI_L}{dt} = V_L \tag{6}$$

where V_C denotes the capacitor's voltage, which equals the output voltage V_{out}.

The dynamics of the capacitor's voltage are governed by the differential equation shown in (7):

$$C\frac{dV_C}{dt} = I_L - I_{load} \tag{7}$$

where I_L is the current through the inductor, and I_{load} is the total current flowing through the RC load, calculated as follows in (8):

$$I_{load} = \frac{V_C}{R} + C\frac{dV_C}{dt} \tag{8}$$

The output of the boost converter, i.e., the RC parallel branch depicted in Figure 3, is connected to a power supply from the EA®-PSB 9000 3U series (EA® Elektro-Automatik, Viersen, Germany) [42]. This power supply, which emulates the behavior of a 350 V Li-Ion battery, imposes the output voltage V_{out} referred to above. This setup functions as a BESS, allowing for operations both as an energy source and a sink. It enables charge and discharge cycles while monitoring and controlling the key indicators of the BESS.

3.2. Layer 2: Measurement

Layer 2 handles the acquisition of voltage and current measurements from the PV array emulator and forwards them to the next layer, the control layer. The sample time T_s considered in this work was 1 ms.

The DACB includes all sensors in this layer: a current transducer for measuring voltage (LEM® LV 25-P) [43] and a non-invasive current sensor (LEM® LA 55-P) [44], both manufactured by LEM® International SA in Geneva, Switzerland. The temperature and irradiance sensors were excluded from the DACB because the platform aims to emulate real conditions within a laboratory environment, not to conduct tests with actual equipment outdoors. Accordingly, the values normally provided by these sensors, T for temperature, and G for irradiance, are artificially generated on the DACB based on historical data relevant to the specified location, as depicted in Table 4. Furthermore, other instruments, such as multimeters and oscilloscopes, were employed to assess voltage and current measurements and to display control signals, respectively.

Table 4. Cases in the proposed sequence, each specifying irradiance levels (W/m^2), operating points, and durations (hours).

Case	Irradiance	Operating Point	Duration (h)
1	900	PRP at 80%	1
2	900	PRP at 60%	1
3	700	PRP at 80%	2
4	500	MPP	2

3.3. Layer 3: Control

Layer 3 enables the PV array emulator to operate at any point within its performance curves, including the MPP or a specified PRP while accounting for variations in temperature and irradiance. To achieve this, Layer 3 employs a hybrid control strategy that combines PI control with an adapted P&O approach. This system integrates the DACB, an Arduino® MEGA (Arduino® SA, Ivrea, Italy) [45], and a custom-developed algorithm programmed on the board.

The systematic approach for controlling the PV array's operating point is depicted in a comprehensive flowchart, as illustrated in Figure 4.

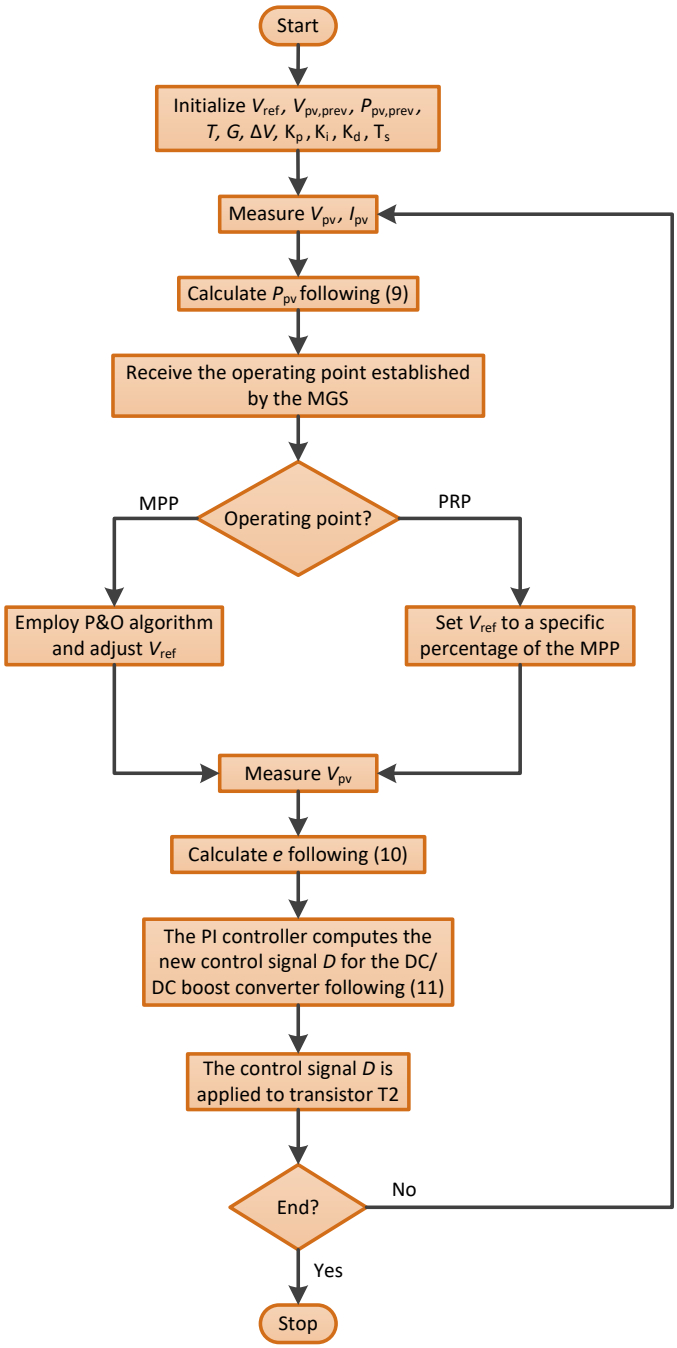

Figure 4. Flowchart illustrating the steps of the hybrid control strategy for controlling the PV array's operating point.

The algorithm begins with the initialization of all necessary parameters. This involves setting the initial reference voltage, V_{ref}, to 3% above the theoretical MPP. This setting represents the starting point for the control system to begin tracking the MPP of the PV array emulator. In addition, it is necessary to initialize the starting values for the previous iteration for both the PV voltage $V_{pv,prev}$ and PV power $P_{pv,prev}$, both of which are set from zero. The temperature T and irradiance G are also provided, depending on the specified case. Regarding the P&O algorithm, it is essential to establish the step size ΔV, set to 0.5% of V_{ref} to represent a small perturbation in voltage as the algorithm progresses. Finally, the PI controller parameters (K_p, K_i, and T_s) are set based on manual tuning, as depicted in Table A2 of Appendix A.

At this stage, the voltage V_{pv} and current I_{pv} of the PV array are measured using the DACB. With these measurements, the power output of the PV array P_{pv} is calculated using (9):

$$P_{pv} = V_{pv} \cdot I_{pv} \tag{9}$$

Next, the MGS establishes how the PV array should operate, whether at the MPP or a specified PRP.

If the system is to operate at the MPP, the P&O algorithm is employed. This algorithm adjusts the reference voltage V_{ref} by comparing the current PV power P_{pv} with the previous PV power $P_{pv,prev}$. If the power increases, V_{ref} is adjusted with a small perturbation ΔV in the same direction; otherwise, the direction is reversed.

If the system is configured to operate at a specified PRP, the reference voltage V_{ref} is adjusted to a value on the P-V curve that corresponds to the reduced power setting. Given that the power at the MPP is known, setting the power reserve at 80% means that the power at the PRP will be 20% less than at the MPP. Consequently, the reference voltage V_{ref} is adjusted to match this reduced power level on the P-V curve.

Subsequently, the output voltage of the PV array V_{pv} is measured. This value should be around the reference voltage V_{ref}. The error signal e for the PI controller is then calculated as (10):

$$e = V_{ref} - V_{pv} \tag{10}$$

Using the error signal, the PI controller calculates the new control signal D, which is then applied to the DC/DC boost converter. As shown in Figure 3, this control signal, identified as S2, is applied to transistor T2. Since the DC/DC boost converter operates with pulse width modulation (PWM), the control signal D determines the duty cycle of the PWM. The control signal is calculated as shown in (11):

$$D[n] = D[n-1] + \mathrm{K_p} \cdot e[n] + \mathrm{K_i} \cdot \sum_{k=0}^{n} e[k] \cdot \mathrm{T_s} \tag{11}$$

where n represents the discrete time step.

The algorithm runs continuously, repeating the process from measuring the PV parameters to updating the control signal until an affirmative end condition is met.

3.4. Layer 4: Communication

Layer 4 provides the MGS with an MGI for configuration and monitoring, as shown in Figure 2. The platform supports two simultaneous processes, both critical to achieving the desired objective: continuous data collection from the PV array emulator and the ability for the MGS to establish the operating point of the PV array emulator at any moment. To facilitate this, full-duplex communication between the DACB and MGI was developed using a Raspberry Pi® 3 Model B+ (Raspberry Pi® Foundation, Cambridge, UK) [46], which serves as the DCB. On the DCB, three Python algorithms were developed to manage these processes: one for each process and another to ensure the simultaneous execution of both.

The algorithm shown in Figure 5 handles continuous data collection from the PV array emulator and transmission to the MGI. Meanwhile, the algorithm in Figure 6 manages the setting of the operating point from the MGS and transmission back to the PV array emulator.

The algorithm illustrated in Figure 5 involves collecting and transmitting data from the PV array emulator to the MGI, facilitated by the DACB and DCB. Specifically, these data include the measured voltage and current from the PV array emulator (V_{pv} and I_{pv}, respectively), the power output P_{pv}, determined as described in (9), the measured reference voltage V_{ref}, and the temperature T and irradiance G that were set. All these parameters are displayed on the MGI.

Initially, the DCB establishes serial communication with the DACB using the RS232 interface, which operates in half-duplex mode. The communication proceeds at a baud rate of 57,600 bps, with data transmitted in a 10-bit frame—consisting of 1 start bit, 8 data bits, and 1 stop bit—in hexadecimal format. Subsequently, the DACB acquires

the mentioned data from the PV array emulator and transmits them back to the DCB via serial communication. The DCB then transmits these data to the MGI via WebSocket, where the DCB acts as the server and the MGI as the client. The algorithm awaits an acknowledgement (ACK) from the MGI to confirm successful data receipt. Upon receiving an ACK, the data are sent and monitored via the MGI. The algorithm repeats this process, from reading data from the PV array emulator to transmitting data to the MGI, until an affirmative end condition is met.

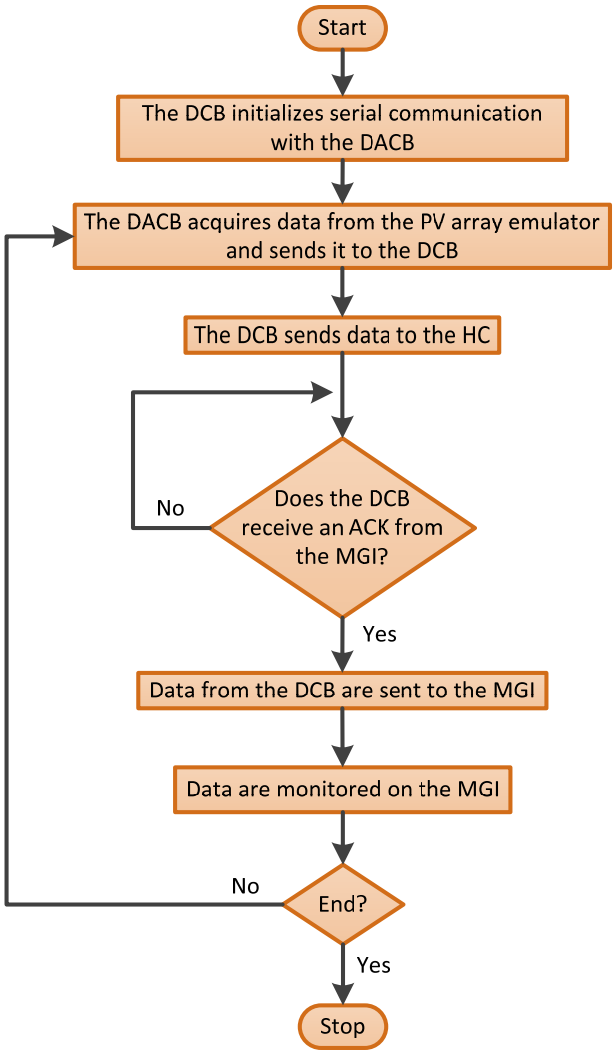

Figure 5. Flowchart illustrating the communication processes for continuously collecting data from the PV array emulator.

The algorithm depicted in Figure 6 is designed to set a sequence of operating points for the PV array emulator, as determined by the MGS.

To start, the DCB establishes serial communication with the DACB. The MGS then configures an initial sequence of operating points, which may vary based on changes in irradiance and temperature. For each point in the sequence, the MGS must specify whether it is the MPP or a designated PRP, along with the corresponding temperature and irradiance levels. During each iteration, the MGI sends the current operating point to the DCB, which then transmits it to the DACB. The algorithm waits for an ACK from the DACB to confirm the successful setting of each operating point in the sequence. Once an ACK is received, the operating point is set for the specified duration. After all points in the sequence are set, the MGS may initiate another sequence. As previously mentioned, changes to an ongoing

sequence are possible, aligning with real-world scenarios where irradiance and temperature fluctuate. The algorithm repeats this process until an end condition is met.

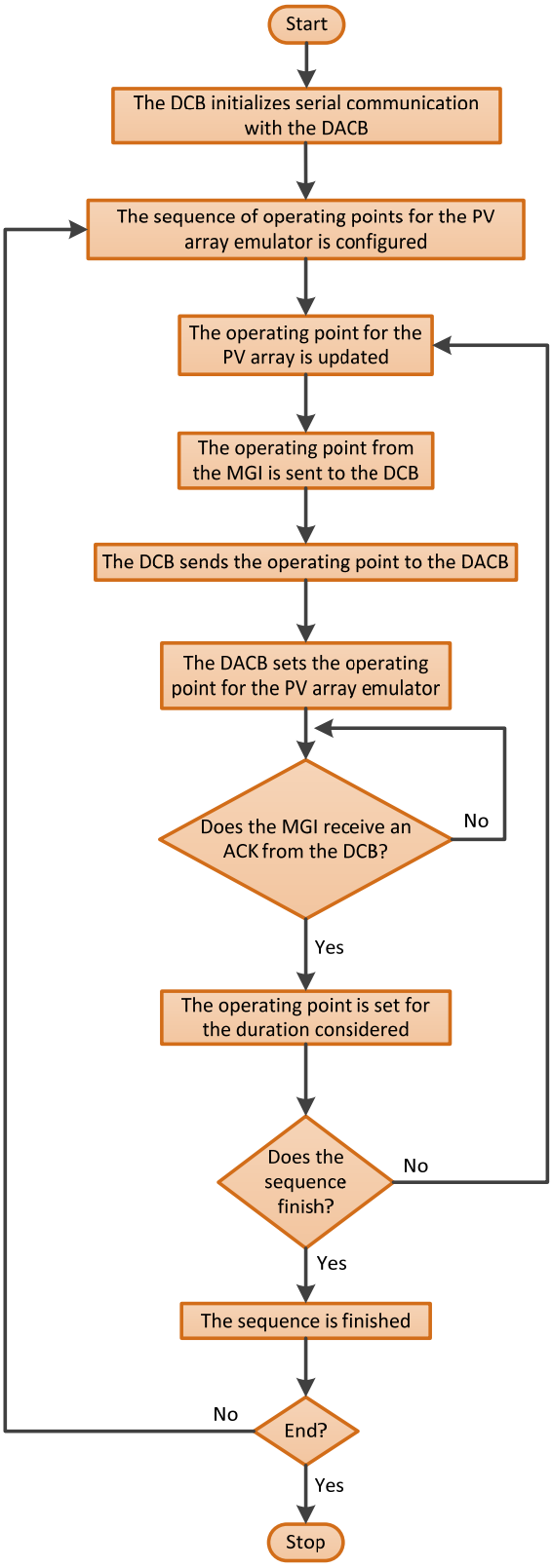

Figure 6. Flowchart illustrating the communication processes used to set a sequence of operating points for the PV array emulator.

3.5. Overview of the Developed Platform

The platform described in the previous subsections is shown in Figure 7. It comprises four layers, each with a specific objective and set of elements. Layer 1 (power) includes the PV array emulator (labeled as 4 in Figure 7) and the DC/DC boost converter (6), consisting of the modular IGBT power stack and electrical components. Layer 2 (measurement) encompasses the DACB (5), the oscilloscope (2), and the multimeters (3). Layer 3 (control) also utilizes the DACB (5), while layer 4 (communication) involves the DCB (5) and the MGI (1). The following section will present the results obtained using this developed platform.

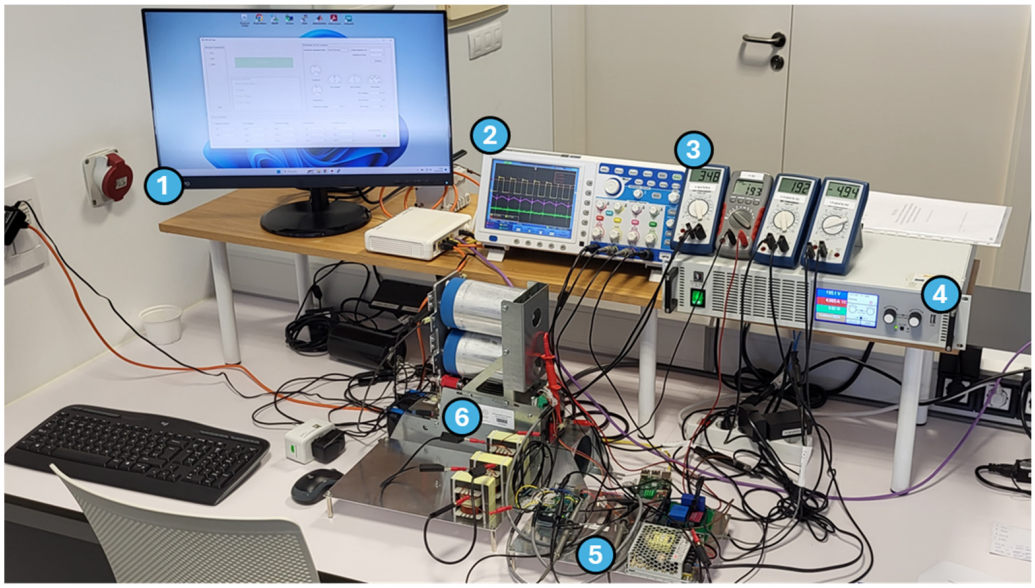

Figure 7. The developed platform used for PV emulation. The numbers in the figure correspond to the following components: 1. MGI, 2. Oscilloscope, 3. Multimeters, 4. PV array emulator, 5. MCC module, consisting of DACB and DCB, 6. DC/DC boost converter.

4. Results

The evaluation methodology focused on assessing the platform's capability to facilitate the integration of PV systems into microgrids. Specifically, it examined the platform's effectiveness in managing operating points, such as MPPs or PRPs, under varying conditions as indicated by the MGS.

Initially, the MGS programmed various operating points for the PV array described in Section 2.2. The objective of this first step was to individually evaluate the deviations between theoretical and experimental power readings for MPPs and PRPs under varying conditions. This was followed by a comparative analysis with findings from other studies.

After assessing how the platform adjusted these operating points, a selection was made based on specific criteria, further explained, to include them in a sequence. This sequence was designed to verify whether the platform could accurately follow the operating points previously specified by the MGS based on predicted generation and demand within a microgrid. This involved an experimental test covering multiple cases. Each case was defined by specific irradiance values, operating points, and durations, as detailed in Table 4. These cases spanned a period from the afternoon to the day's end, when irradiance typically decreases, representing a typical daily scenario for the proposed evaluation. Standard values from the literature [47] were used to select the values for irradiance and power reserve. It is important to note that, in reality, irradiance levels do not remain constant over the duration considered. For instance, in case 1, an irradiance of 900 W/m^2 would not be constant for one hour. This is a simplification, and thus, this approach is applicable only under simulated or emulated conditions. To evaluate the platform's ability to follow the established sequence, theoretical and experimental power values were compared.

The irradiance and temperature values used in the experimental setup were artificially generated based on historical data specific to the location. Table 4 presents the irradiance values for the proposed cases, while the temperature value was kept constant at 25 °C for all cases. This is because, in real-world applications, temperature fluctuations generally occur more gradually compared to the rapid and often challenging changes in irradiance, such as those caused by shading conditions. It is important to note that the MPP value shown in Table 3 corresponds to T = 25 °C and I = 1000 W/m^2. Consequently, as the irradiance varies in the proposed cases, the MPP shifts according to the theoretical performance curves of the selected PV array.

The results are detailed in the following subsections.

4.1. Performance in Adjusting Operating Points

In this subsection, the MGS programmed various operating points for the selected PV array, following the steps outlined in Figure 6. The objective was to evaluate the platform's ability to adjust to different operating points, characterized by irradiance values of 900, 700, and 500 W/m^2, a constant temperature of 25 °C, and operating points at both MPP and PRP at 80% and 60%. To conduct the evaluation, the deviations between the theoretical and experimental power readings were analyzed.

The theoretical I-V and P-V curves of the selected PV array were simulated based on its mathematical model, as described in Section 2.1.1, using the parameters provided in Tables 2 and 3. Both curves are shown in Figure 8 under the specified irradiance levels.

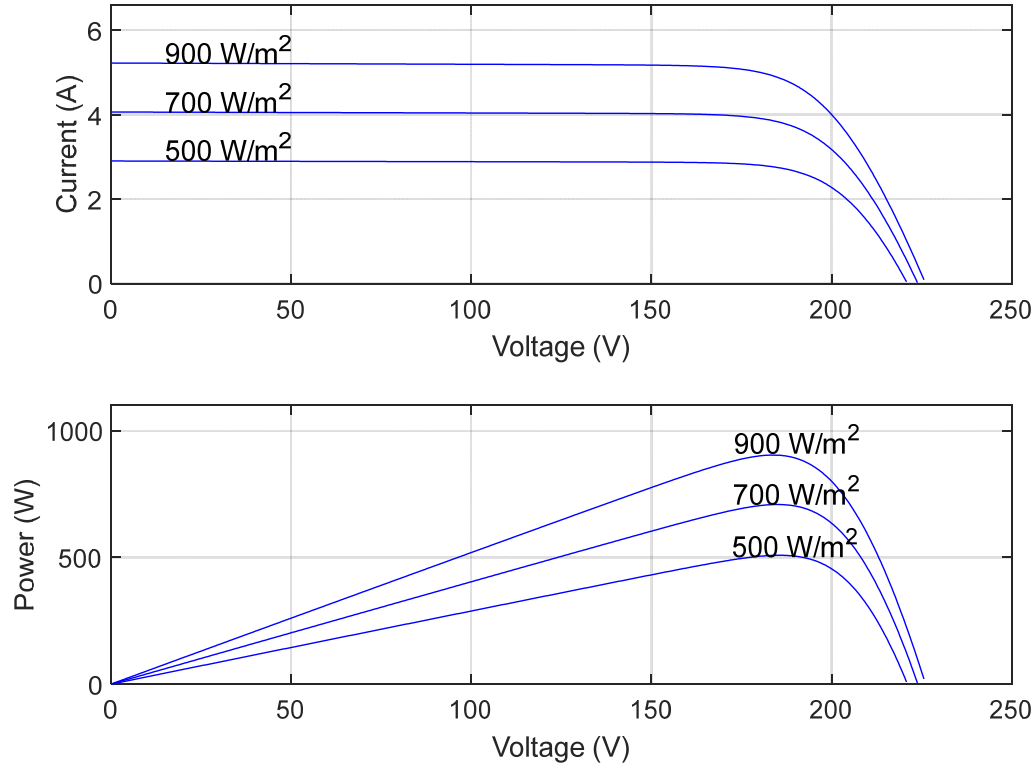

Figure 8. I-V and P-V curves of the selected PV array at 25 °C and irradiance levels of 500, 700, and 900 W/m^2.

Figure 9 highlights the differences between theoretical operating points, derived from the 1M5P model as the ideal values, and the experimental operating points, obtained using the developed platform. It is important to note that we used the 1M5P model because it is the model used for the PV emulator.

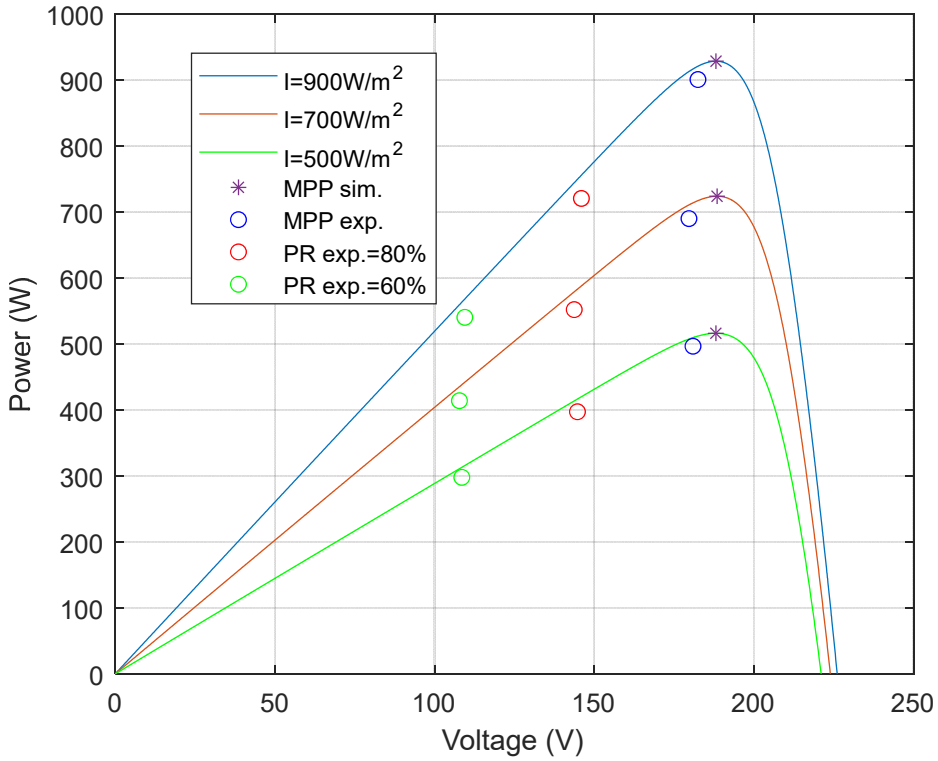

Figure 9. P-V curves of the selected PV array under varying irradiance levels, with the identification of the theoretical MPP (MPP sim.) and experimental MPP (MPP exp.), as well as experimental PR (PR exp.) points at 80% and 60% on each curve.

In addition, Table 5 presents the deviations in power output between theoretical and experimental values for each irradiance level shown in Figure 9. It is important to note that the power deviation represents the average for all operating points within the same irradiance level.

Table 5. Comparison of power deviations for the identified cases in Figure 9.

Irradiance	Operating Point	Power Deviation
900	MPP PR = 80% PR = 60%	3%
700	MPP PR = 80% PR = 60%	4.67%
500	MPP PR = 80% PR = 60%	3.81%

Moreover, an oscilloscope was used to verify the signals from the developed platform, as shown in Figure 10. The red trace displays S2, which is the control signal applied to transistor T2 (see Figure 3). This signal exhibits the typical square-wave characteristics of a PWM signal, controlling the transistor's switching actions. The yellow trace illustrates the voltage across transistor T2, indicating its on–off states. The purple trace represents the current sensor voltage from the PV array emulator, exhibiting a sawtooth pattern that captures the inductor current's response to the transistor's switching, influenced by the control signal for the DC/DC boost converter. Lastly, the green trace indicates the voltage sensor output from the PV array emulator.

Figure 10. Signals representing the control signal applied to transistor T2 (red trace), the voltage across transistor T2 (yellow trace), the current sensor voltage from the PV array emulator (purple trace), and the voltage sensor output from the PV array emulator (green trace). All signals are measured in V.

4.2. Performance in Following Operating Point Sequences

In this subsection, selected operating points identified in Figure 9, along with their durations, were incorporated into a sequence based on the criteria outlined in Section 2.2, reflecting typical daily operations in a PV system. This approach allowed for the evaluation of the platform's capability to manage a sequence of operating points, assessing its potential to facilitate the integration of PV systems into microgrids.

The sequence proposed in Table 4 was executed to compare the theoretical and experimental power outputs for each case in the sequence. The results of applying this sequence to the PV array emulator are shown in Figure 11, which displays both the theoretical and experimental power across the duration considered. It is important to note that each transition depicted in Figure 11 corresponds to a case change, as detailed in Table 4.

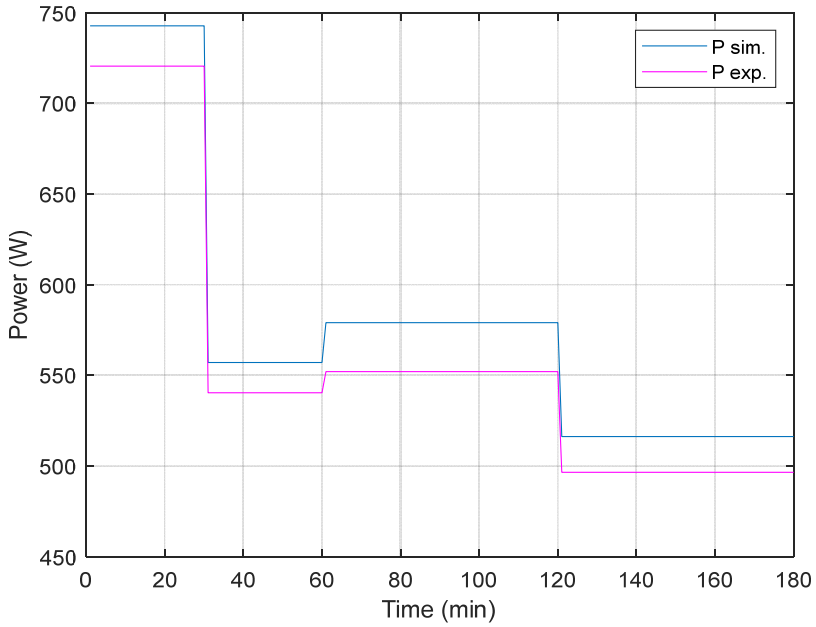

Figure 11. Comparison of theoretical power output (P sim.) and experimental power output (P exp.) of the selected PV array for the cases considered in Table 4.

5. Discussion

5.1. Performance in Adjusting Operating Points

Figure 8 shows the I-V and P-V curves for the selected PV array, demonstrating behavior consistent with typical patterns [48]. As irradiance decreases, the MPP shifts to lower power and current levels.

Figure 9 and Table 5 offer a visual and analytical discussion, respectively, of the performance of the developed platform in adjusting the operating point of the PV array emulator. Figure 9 illustrates the alignment between the theoretical and experimental MPPs, with the PRPs closely surrounding the P-V curve. Notably, all experimental points lie below the P-V curve, indicating that experimental power is lower than theoretical power—a common occurrence in real-world scenarios [49]. Table 5 provides a detailed comparison of the deviations between theoretical and experimental power outputs across different irradiance levels. The deviations generally range between 3% and 4.67%, demonstrating that experimental results closely approximate theoretical values. This conclusion is based on the evaluation of nine operating points with varying irradiance levels, as shown in Figure 9, which are most relevant to the intended application, as outlined in Section 4. However, several operating points under various temperature and irradiance conditions were tested.

At an irradiance of 900 W/m^2, a minimal deviation of only 3% is observed. When the irradiance is reduced to 700 W/m^2, the deviation at the MPP increases to 4.67%, suggesting a decrease in power output accuracy at lower irradiance levels. The lowest irradiance level considered, 500 W/m^2, shows a deviation of 3.81%. The mean power deviation across all tested irradiance levels is calculated at 3.83%, with the maximum power deviation reaching 4.67%, highlighting slight differences. These values, falling within the typical efficiency range of 95% to 98%, are considered acceptable [50]. It is important to note that each power deviation value shown in Table 5 represents the average of deviations across different operating points at a given irradiance level. This approach was chosen because the power deviation values for the various operating points under the same irradiance value were similar, facilitating further analysis. Despite these minor variations, the minimal deviations detailed in Table 5 highlight the platform's consistent performance across different settings.

The signals displayed in Figure 10 show the dynamic behavior of key points in the developed platform, including the PWM signal (red trace), the voltage across T2 (yellow trace), the current sensor voltage from the PV array emulator (purple trace) and the voltage sensor output from the PV array emulator (green trace). The red and yellow traces confirm the effective switching operation of transistor T2, controlled by the PWM signal generated by the DACB. The purple and green traces provide insights into the inductor current and output voltage behaviors, respectively. Specifically, the alternating pattern of the purple trace is crucial as it confirms the DC-DC boost converter's response to control adjustments, and the slight noise level of the green trace suggests the potential need for improved voltage sensing methods or better filtering to achieve more stable output voltage.

In summary, the results showed that the operating points adjusted by the platform deviated by no more than 5% from theoretical values, highlighting the platform's potential for managing operating points in PV systems. This achievement serves as the foundation for the next assessment: evaluating whether the platform can effectively follow a sequence of operating points.

5.2. Performance in Following Operating Point Sequences

Figure 11 visually compares the platform's adherence to the sequence of operating points defined in Table 4, specifically evaluating the communication process used to establish these operating points, as detailed in Figure 6.

This comparison highlights the platform's ability to match the proposed sequence, showing that the deviations between the theoretical and experimental results, as observed in Figure 11, fall within an acceptable range because the cases conducted are some of the selected in Section 5.1. This not only demonstrates the platform's capability to precisely

control the operating point of the PV array in a sequence but also emphasizes the reliability of the communication process between the MGI and the PV array emulator in executing the necessary command sequences. Allowing the MGS to select a sequence of operating points for PV systems aligns the development with real-world scenarios and offers a more automated method of control.

In summary, the results demonstrate the platform's capability to effectively manage the operating points of a PV array according to a predefined sequence, thereby facilitating the integration of PV systems into microgrids.

6. Conclusions

Photovoltaic solar energy plays a crucial role in the global transition toward decarbonization, making PV systems indispensable for capturing solar power. Integrating these systems into microgrids is essential for increasing the share of renewable energy in the overall energy mix, thereby reducing reliance on fossil fuels. However, this integration presents significant challenges, including the variability of photovoltaic solar energy production, the need for efficient energy management, and the complexities involved in grid synchronization and communication between all components.

PV emulator platforms have emerged as powerful tools to provide effective solutions to these challenges, enabling the precise management of the PV array's operating points in a controlled environment. This allows for the replication of a wide range of power outputs and environmental conditions without geographic or meteorological constraints.

Despite progress, existing PV emulator platforms often lack comprehensive integration of measurement, control, and communication capabilities, as well as a controllable environment for varying operating conditions, limiting their effectiveness in microgrid scenarios.

This paper presents a PV emulator platform designed to address these gaps by integrating power systems, real-time control systems, measurement instrumentation, and communication processes. These integrated features enable precise emulation of PV behavior under various operating conditions. The platform ensures reliable operation at critical points such as the MPP or a specified PRP, and its integration with other microgrid components is seamless. Furthermore, its capacity to adjust and follow sequences of operating points significantly enhances its dynamic energy management capabilities within microgrid applications.

The platform demonstrated a high level of performance, with efficiency ranging from 95% to 98%, and successfully followed sequences of operating points, significantly improving the integration of PV systems into microgrids.

While the current development of the platform does not consider the impact of shading on PV systems, this aspect may be addressed in future work to enhance the platform's applicability.

The platform benefits various stakeholders by improving system efficiency and stability while also serving as an educational tool for understanding PV system operation. For microgrid operators, it offers a valuable tool for remote monitoring and energy optimization, particularly in isolated microgrids where consistent energy access is critical. End-users enjoy more reliable and cost-effective energy solutions, while academic institutions can utilize this platform to enrich solar technology education and research.

Finally, the contributions of this work are twofold. First, it advances the field of photovoltaic solar energy research, particularly in the study of PV systems. Second, it provides a practical tool that enhances the design and management of PV systems within microgrid environments, furthering the path to decarbonization.

Author Contributions: Conceptualization, G.G.-R. and R.S.-H.; methodology, G.G.-R. and R.S.-H.; software, G.G.-R. and J.M.C.; validation, G.G.-R., R.S.-H., J.M.C. and J.C.-C.; formal analysis, G.G.-R. and R.S.-H.; investigation, G.G.-R. and R.S.-H.; resources, R.S.-H. and F.J.R.-R.; data curation, G.G.-R., R.S.-H. and J.C.-C.; writing—original draft preparation, G.G.-R.; writing—review and editing, R.S.-H. and J.M.A.; visualization, G.G.-R. and R.S.-H.; supervision, R.S.-H. and J.M.A.; project administration, R.S.-H.; funding acquisition, R.S.-H. All authors have read and agreed to the published version of the manuscript.

Funding: This paper is part of the project "Integral control system to optimize the microgrids energy demand", grant number PID2020-117828RB-I00, funded by the Spanish Ministry of Science, Innovation and Universities. The author Gabriel Gómez-Ruiz is enjoying an FPU grant, number FPU21/00468, funded by the Spanish Ministry of Science, Innovation and Universities for the training of university teaching staff during his PhD period. The author Jesús Clavijo-Camacho has benefited from an INVESTIGO research fellowship funded by the European Union-NextGenerationEU.

Data Availability Statement: The data presented in this study are available upon request from the corresponding author.

Conflicts of Interest: The authors declare no conflicts of interest.

Appendix A. Related to the Developed PV Emulator Platform

Table A1. Parameters involved in the DC/DC boost converter.

Parameter	Value
R	68 kΩ
L	6.8 mH
C	850 μF

Table A2. PI controller parameters.

Parameter	Value	Unit
K_p	7	-
K_i	0.003	-
T_s	0.001	s

References

1. Wang, Z.; Li, S.; Jin, Z.; Li, Z.; Liu, Q.; Zhang, K. Oil and Gas Pathway to Net-Zero: Review and Outlook. *Energy Strategy Rev.* **2023**, *45*, 101048. [CrossRef]
2. 2050 Long-Term Strategy. Available online: https://climate.ec.europa.eu/eu-action/climate-strategies-targets/2050-long-term-strategy_en (accessed on 11 July 2023).
3. Ritchie, H.; Roser, M.; Rosado, P. Energy Mix. *Our World Data*. 2022. Available online: https://ourworldindata.org/energy-mix (accessed on 8 September 2023).
4. Rodriguez, M.; Arcos-Aviles, D.; Martinez, W. Fuzzy Logic-Based Energy Management for Isolated Microgrid Using Meta-Heuristic Optimization Algorithms. *Appl. Energy* **2023**, *335*, 120771. [CrossRef]
5. Youssfi, A.; Alioui, A.; Kadi, Y.A.E. Study, Simulation and Realization of a Fuzzy Logic-Based MPPT Controller in an Isolated DC Microgrid. *Indones. J. Electr. Eng. Comput. Sci.* **2024**, *34*, 1420–1433. [CrossRef]
6. Obaideen, K.; Olabi, A.G.; Al Swailmeen, Y.; Shehata, N.; Abdelkareem, M.A.; Alami, A.H.; Rodriguez, C.; Sayed, E.T. Solar Energy: Applications, Trends Analysis, Bibliometric Analysis and Research Contribution to Sustainable Development Goals (SDGs). *Sustainability* **2023**, *15*, 1418. [CrossRef]
7. Mansouri, N.; Lashab, A.; Sera, D.; Guerrero, J.M.; Cherif, A. Large Photovoltaic Power Plants Integration: A Review of Challenges and Solutions. *Energies* **2019**, *12*, 3798. [CrossRef]
8. Shaher, A.; Alqahtani, S.; Garada, A.; Cipcigan, L. Technical Potential for Rooftop Solar Photovoltaic in Commercial and Residential Areas in Saudi Arabia. In Proceedings of the 2022 57th International Universities Power Engineering Conference (UPEC), Istanbul, Turkey, 30 August–2 September 2022; pp. 1–6.
9. Hassan, Q.; Abdulrahman, I.S.; Salman, H.M.; Olapade, O.T.; Jaszczur, M. Techno-Economic Assessment of Green Hydrogen Production by an Off-Grid Photovoltaic Energy System. *Energies* **2023**, *16*, 744. [CrossRef]
10. Mohsen, M.S.; Jaber, J.O. A Photovoltaic-Powered System for Water Desalination. *Desalination* **2001**, *138*, 129–136. [CrossRef]
11. Marques Lameirinhas, R.A.; Torres, J.P.N.; de Melo Cunha, J.P. A Photovoltaic Technology Review: History, Fundamentals and Applications. *Energies* **2022**, *15*, 1823. [CrossRef]
12. de Melo Bento, A.A.; Perci Santiago, R. A Low Cost Photovoltaic Panel Emulator. In Proceedings of the 2019 IEEE 15th Brazilian Power Electronics Conference and 5th IEEE Southern Power Electronics Conference (COBEP/SPEC), Santos, Brazil, 1–4 December 2019; pp. 1–5.
13. Schweiger, M.; Herrmann, W.; Gerber, A.; Rau, U. Understanding the Energy Yield of Photovoltaic Modules in Different Climates by Linear Performance Loss Analysis of the Module Performance Ratio. *IET Renew. Power Gener.* **2017**, *11*, 558–565. [CrossRef]
14. Elgendy, M.A.; Zahawi, B.; Atkinson, D.J. Operating Characteristics of the P&O Algorithm at High Perturbation Frequencies for Standalone PV Systems. *IEEE Trans. Energy Convers.* **2015**, *30*, 189–198. [CrossRef]

15. Dhaouadi, G.; Djamel, O.; Youcef, S.; Salah, C. Implementation of Incremental Conductance Based MPPT Algorithm for Photovoltaic System. In Proceedings of the 2019 4th International Conference on Power Electronics and their Applications (ICPEA), Elazig, Turkey, 25–27 September 2019; pp. 1–5.
16. Lasheen, M.; Abdel Rahman, A.K.; Abdel-Salam, M.; Ookawara, S. Adaptive Reference Voltage-Based MPPT Technique for PV Applications. *IET Renew. Power Gener.* **2017**, *11*, 715–722. [CrossRef]
17. Elgendy, M.A.; Zahawi, B.; Atkinson, D.J. Evaluation of Perturb and Observe MPPT Algorithm Implementation Techniques. In Proceedings of the 6th IET International Conference on Power Electronics, Machines and Drives (PEMD 2012), Bristol, UK, 27–29 March 2012; pp. 1–6.
18. Sampaio, L.P.; Oliveira da Silva, S.A. Graphic Computational Platform Integrated with an Electronic Emulator Dedicated to Photovoltaic Systems Teaching. *IET Power Electron.* **2017**, *10*, 1982–1992. [CrossRef]
19. Harris, M.J.; Christenson, R.E. Real-Time Hybrid Simulation Using Analogue Electronic Computer Technology. *Int. J. Lifecycle Perform. Eng.* **2020**, *4*, 25–45. [CrossRef]
20. Mishra, S.; Raju, S.; Kshirsagar, A.; Mohan, N. An Extremely Low-Cost Multi-Panel PV Emulator for Research and Education. In Proceedings of the 2018 IEEE Energy Conversion Congress and Exposition (ECCE), Portland, OR, USA, 23–27 September 2018; pp. 4760–4765.
21. Khawaldeh, H.A.; Al-Soeidat, M.; Lu, D.D.-C.; Li, L. Accurate, Fast and Power Efficient PV Emulator Based on Hybrid Passive and Active Circuits. *CPSS Trans. Power Electron. Appl.* **2022**, *7*, 432–441. [CrossRef]
22. Alaoui, M.; Maker, H.; Mouhsen, A.; Hihi, H. Real-Time Emulation of Photovoltaic Energy Using Adaptive State Feedback Control. *SN Appl. Sci.* **2020**, *2*, 492. [CrossRef]
23. Estrada, L.; Vazquez, N.; Ortega, J.; López, H.; Hernández, C.; Vaquero, J. Low Cost PV Emulator Based on Programmable DC Power Supply and LabVIEW. In Proceedings of the IECON 2021—47th Annual Conference of the IEEE Industrial Electronics Society, Toronto, ON, Canada, 13–16 October 2021; pp. 1–6.
24. Jayawardana, I.; Ho, C.N.M. A Power Electronics-Based Power HIL Real Time Simulation Platform for Evaluating PV-BES Converters on DC Microgrids. In Proceedings of the 2021 IEEE Energy Conversion Congress and Exposition (ECCE), Vancouver, BC, Canada, 10–14 October 2021; pp. 688–693.
25. Guo, L.; Kors, J. Design of a Laboratory Scale Solar Microgrid Cyber-Physical System for Education. *Electronics* **2021**, *10*, 1562. [CrossRef]
26. Xiong, X.; Yang, Y. A Photovoltaic-Based DC Microgrid System: Analysis, Design and Experimental Results. *Electronics* **2020**, *9*, 941. [CrossRef]
27. Moussa, I.; Khedher, A.; Bouallegue, A. Design of a Low-Cost PV Emulator Applied for PVECS. *Electronics* **2019**, *8*, 232. [CrossRef]
28. Posada Contreras, J.; Rosas-Caro, J.C. Hardware-in-the-Loop Emulation of a SEPIC Multiplier Converter in a Photovoltaic System. *Electricity* **2024**, *5*, 426–448. [CrossRef]
29. Korasiak, P.; Jaglarz, J. A New Photovoltaic Emulator Designed for Testing Low-Power Inverters Connected to the LV Grid. *Energies* **2022**, *15*, 2646. [CrossRef]
30. Saraswathi, K.T.; Arumugam, P.; Swaminathan, G.V.; Periasamy, S. An Artificial Neural Network-Based Comprehensive Solar Photovoltaic Emulator. *Int. J. Photoenergy* **2022**, *2022*, 4741428. [CrossRef]
31. Chavarria, J.; Biel, D.; Guinjoan, F.; Poveda, A.; Masana, F.; Alarcon, E. Low Cost Photovoltaic Array Emulator Design for the Test of PV Grid-Connected Inverters. In Proceedings of the 2014 IEEE 11th International Multi-Conference on Systems, Signals & Devices (SSD14), Barcelona, Spain, 11–14 February 2014; pp. 1–6.
32. Clavijo-Camacho, J.; Gomez-Ruiz, G.; Ruiz-Rodriguez, F.J.; Sanchez-Herrera, R. A Modular IGBT Power Stack—Based and Open Hardware Framework for Small Wind Turbines Assessment. *Sustain. Energy Technol. Assess.* **2024**, *66*, 103804. [CrossRef]
33. Marquez, M.A.; Herrera, R.S.; Mejias, A.; Esquembre, F.; Andujar, J.M. Controlled and Secure Access to Promote the Industrial Internet of Things. *IEEE Access* **2018**, *6*, 48289–48299. [CrossRef]
34. Sánchez-Herrera, M.R.; Márquez, M.; de la Torre, L. Secure and Private Internet of Things for Industry, Training, and Homes: A Communications Solution for Connected Devices. *IEEE Ind. Electron. Mag.* **2023**, *17*, 14–21. [CrossRef]
35. Solar Photovoltaic Cell Basics. Available online: https://www.energy.gov/eere/solar/solar-photovoltaic-cell-basics (accessed on 29 June 2024).
36. Implement PV Array Modules-Simulink-MathWorks España. Available online: https://es.mathworks.com/help/sps/powersys/ref/pvarray.html (accessed on 25 July 2024).
37. Cano, J.M.; Martin, A.D.; Herrera, R.S.; Vazquez, J.R.; Ruiz-Rodriguez, F.J. Grid-Connected PV Systems Controlled by Sliding via Wireless Communication. *Energies* **2021**, *14*, 1931. [CrossRef]
38. Martin, A.D.; Cano, J.M.; Herrera, R.S.; Vazquez, J.R. Wireless Sliding MPPT Control of Photovoltaic Systems in Distributed Generation Systems. *Energies* **2019**, *12*, 3226. [CrossRef]
39. Cano, J.M.; Herrera, R.S.; Martin, A.D.; Vazquez, J.R. Complete and Versatile Remote Controller for PV Systems. *Int. J. Electr. Power Energy Syst.* **2022**, *142*, 108324. [CrossRef]
40. EA-PSI 9360-15. Available online: https://elektroautomatik.com/shop/es/productos/fuentes-de-alimentacion-dc-programables-de-laboratorio/serie-discontinuada/serie-psi-9000-2u-1-kw-hasta-3-kw/558/laboratory-power-supply-0.360v/0..15a (accessed on 2 October 2023).

41. Romera, X. Montajes IGBT de Media Potencia-Rectificadores Guasch, S.A. *Rectificadores Guasch SAU*. Available online: https://www.e-guasch.com/es/power-electronics-items/montajes-igbt-media-potencia/ (accessed on 16 June 2024).
42. EA-PSB 9000 3U. Available online: https://elektroautomatik.com/shop/es/productos/fuentes-de-alimentacion-dc-programables-de-laboratorio/fuentes-de-alimentacion-dc-bidireccionales-de-laboratorio/fuentes-de-alimentacion-dc-bidireccionales-de-laboratorio-psb-9000-3u/832/bi-directional-power-supply (accessed on 16 June 2024).
43. LV 25-P | LV25 | Closed Loop Hall Effect. Available online: https://www.lem.com/en/product-list/lv-25p (accessed on 2 September 2024).
44. LA 55-P | LA55 | Closed Loop Hall Effect. Available online: https://www.lem.com/en/product-list/la-55p (accessed on 2 September 2024).
45. Arduino Mega 2560 Rev3—Arduino Official Store. Available online: https://store.arduino.cc/products/arduino-mega-2560-rev3 (accessed on 17 June 2024).
46. Buy a Raspberry Pi 3 Model B+—Raspberry Pi. Available online: https://www.raspberrypi.com/products/raspberry-pi-3-model-b-plus/ (accessed on 18 June 2024).
47. Batzelis, E.I.; Kampitsis, G.E.; Papathanassiou, S.A. Power Reserves Control for PV Systems With Real-Time MPP Estimation via Curve Fitting. *IEEE Trans. Sustain. Energy* **2017**, *8*, 1269–1280. [CrossRef]
48. Tian, H.; Mancilla-David, F.; Ellis, K.; Muljadi, E.; Jenkins, P. A Cell-to-Module-to-Array Detailed Model for Photovoltaic Panels. *Sol. Energy* **2012**, *86*, 2695–2706. [CrossRef]
49. Peng, J.; Lu, L.; Yang, H.; Ho, K.M.; Law, P. Experimentally Diagnosing the Shading Impact on the Power Performance of a PV System in Hong Kong. In Proceedings of the 2013 World Congress on Sustainable Technologies (WCST), London, UK, 9–12 December 2013; pp. 18–22.
50. De Brito, M.A.G.; Galotto, L.; Sampaio, L.P.; Melo, G.D.A.E.; Canesin, C.A. Evaluation of the Main MPPT Techniques for Photovoltaic Applications. *IEEE Trans. Ind. Electron.* **2013**, *60*, 1156–1167. [CrossRef]